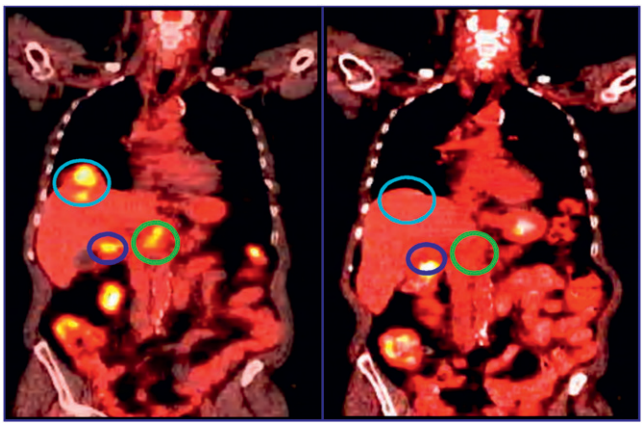

FIGURE 18. PET/CT imaging at baseline (left) and 4 wk after (right) fractionated radioimmunotherapy with ^{90}Y-clivatuzumab tetraxetan plus gemcitabine in advanced pancreatic cancer. Treatment response is highlighted in large liver lesion (light blue), portacaval lymph nodes (dark blue), and primary pancreatic tumor (green).

(New York, NY), a consortium of universities and medical centers, and Immunomedics, Inc. (Morris Plains, NY), reported on "Fractionated RIT with ^{90}Y-clivatuzumab tetraxetan (^{90}Y-PAM4) plus gemcitabine (Gem) in advanced pancreatic cancer" [357]. Figure 18 shows uptake with FDG before treatment and 4 wk after treatment in a patient. The study included 38 patients, 58% of whom survived ≥ 6 mo, 26% ≥ 12 mo, and 5 of whom were still alive 15–25 mo from start of treatment.

Conclusion

It is challenging to look ahead and pick the winners from the more than 130 new tracers presented at this meeting. The following have great promise: ^{68}Ga-bombesin–like peptides in prostate; ^{18}F-glutamine, which reflects novel metabolomics, and other novel glutamine tracers; ^{18}F-DCFBC, which targets PSMA; new small molecules for reliable targeting; and optical imaging alone and in combinations. The Warburg effect is a powerful window on the biology of human cancer for diagnosis and staging and for biomarkers in treatment response. I would urge the cancer imaging community to do a better job in organizing true studies that are adequately powered so that we can meet the high bar the FDA has set in terms of first validating tracers as to reproducibility and next qualifying them for specific uses. This is different from staging and detection—this is looking at treatment response. We can do this as a professional society if we work together with other organizations.

Other substrates, including ^{18}F-choline, ^{11}C-choline, and ^{18}F-amino acids, may add to our capabilities, as well as new radiotracers for cancer pharmacology. We are moving toward individualized treatment based on highly individualized imaging. Imaging biomarker studies are in their infancy, but we are beginning to see emerging efforts to define novel response parameters that go beyond the Response Evaluation Criteria in Solid Tumors. We need a data-based consensus on functional response parameters, including definition of these parameters and ways to design the studies.

Exploration of antibodies and variants, peptides, affibodies, and other platforms, especially with PET nuclides, is expanding. Multistep RIT is showing its advantages for therapeutic index, and I believe that targeted radiotherapy is a big part of our future. We must continue to push forward the good drugs like Bexxar and point out to our colleagues that these are excellent drugs for specific purposes. We must overcome the economic disadvantages of these compounds and promote their clinical advantages so that they are introduced and used widely. Encouraging results in radioresistant solid tumors also offer near-term possibilities that merit further exploration.

Steven M. Larson, MD
Memorial Sloan–Kettering Cancer Center
New York, New York

General Nuclear Medicine

The Scientific Program Committee (SPC) accepted 215 abstracts in the category of general nuclear medicine for this Annual Meeting. The SPC defines general nuclear medicine into subcategories that one would expect (endocrinology, gastroenterology, hematology/infectious disease, musculoskeletal, pediatrics, pulmonary, renal/hypertension, operations/outcomes research); however, it also includes ones that might not be expected (oncology, ^{18}F-FDG, and therapy currently in clinical practice).

Bone SPECT/CT

Last year I highlighted a number of presentations on bone SPECT/CT. Hassan et al. from Guy's and St. Thomas Hospital National Health Trust (London, UK) this year had 2 presentations on bone SPECT/CT: "The potential role of radionuclide bone SPECT/CT in patients with complicated painful knees" [514] and the "Role of ^{99m}Tc-MDP bone SPECT/CT in localization, diagnosis, and treatment of patients with wrist pain." The knee study included 35 patients, and the wrist study included 53 patients. The authors found that bone SPECT/CT was superior to planar imaging at localizing, characterizing, and guiding disease management. Figure 19 is an example of a patient with bilateral amputations and suspected osteomyelitis. The whole-body bone scan could not differentiate between soft tissue and bone uptake. SPECT suggested that the uptake was superficial; the SPECT/CT fused image confirmed that this was soft tissue and corresponded to heterotopic ossification seen on CT. Another example (Fig. 20) illustrates a patient with bilateral renal transplants, on steroids, with bilateral knee pain. SPECT/CT clearly demonstrated that the nondescript focal knee uptake seen on planar and SPECT images was localized to the femoral condyles and not soft tissue, suggesting the diagnosis of bilateral avascular necrosis, which was later confirmed.

Harvey A. Ziessman, MD

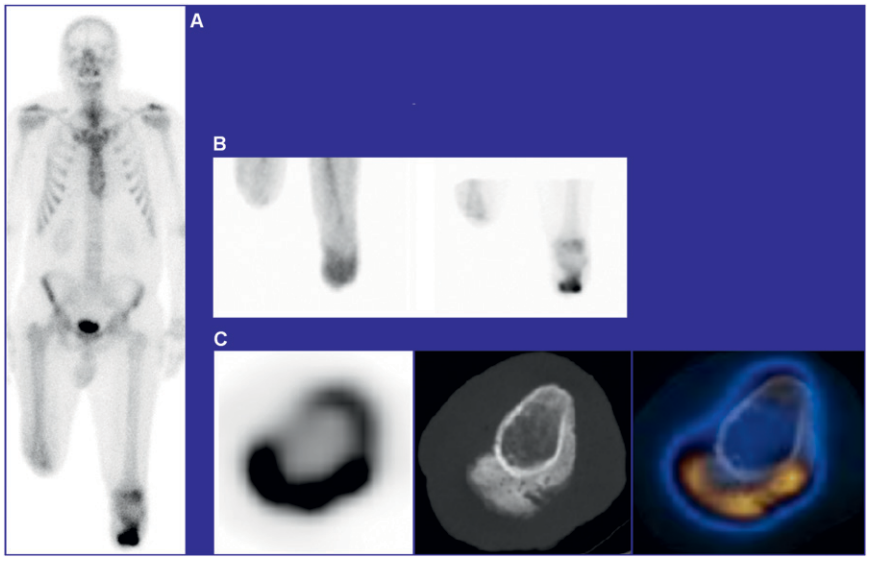

FIGURE 19. Bilateral amputations, bone vs. soft tissue infection. Left: Whole-body imaging. Top: Blood pool (left) and delayed (right) imaging. Bottom: SPECT (left); CT (middle); fused (right) images showing uptake corresponding to heterotophic ossification.

"The role of SPECT/CT in imaging of the Charcot foot" was presented by D'Sa et al. from Kings College (London, UK). The investigators studied 14 diabetic patients who had red swollen feet suggestive of Charcot joints. They found that 11 patients had findings of Charcot joint, and 3 had fractures. Figure 21 shows 2 different patient studies that confirm the utility of SPECT/CT.

Interest is growing in the use of ^{18}F-sodium fluoride (^{18}F-NaF). Drubach and Laffin from Children's Hospital (Boston, MA) reported on "Bone scintigraphy with ^{18}F-NaF in children." The study included 450 patients referred from sports medicine with back pain and suspected stress fractures and 50 patients in whom child abuse was suspected. Figure 22 shows 3 children with traumatic spine injuries, where ^{18}F-NaF PET confirmed equivocal findings or detected new findings not seen on skeletal survey. In the group of patients with suspected child abuse, the authors showed an improved sensitivity with ^{18}F-NaF PET in fractures when compared with skeletal survey (85% and 72%, respectively). ^{18}F-NaF PET was less sensitive than skeletal survey in patients with chronic myelogenous leukemia (67% and 80%, respectively).

Quon et al. from Stanford University School of Medicine (CA) and Hospital Mãe de Deus (Porto Alegre, Brazil) reported on "Integrated ^{18}F-NaF PET/CT scanning for the evaluation of recurrent pain after spinal fixation surgery." They prospectively studied 21 patients with equivocal CT/MR imaging findings. Based on the ^{18}F-NaF PET/CT findings, 14 patients were recommended for surgical exploration and 7 patients for noninvasive therapy. ^{18}F-NaF PET/CT had a positive predictive value (PPV) of 93% and a negative predictive value (NPV) of 100%. Focal uptake correlated with surgical findings of hardware failure, screw loosening, graft failure, and spine instability (83% PPV). Figure 23 shows a patient with a cervical spine fixation device. The maximum-intensity projection (MIP) image showed abnormal uptake localized to the proximal and distal ends of the fixation hardware, which correlated with surgical identification of hardware loosening at these sites.

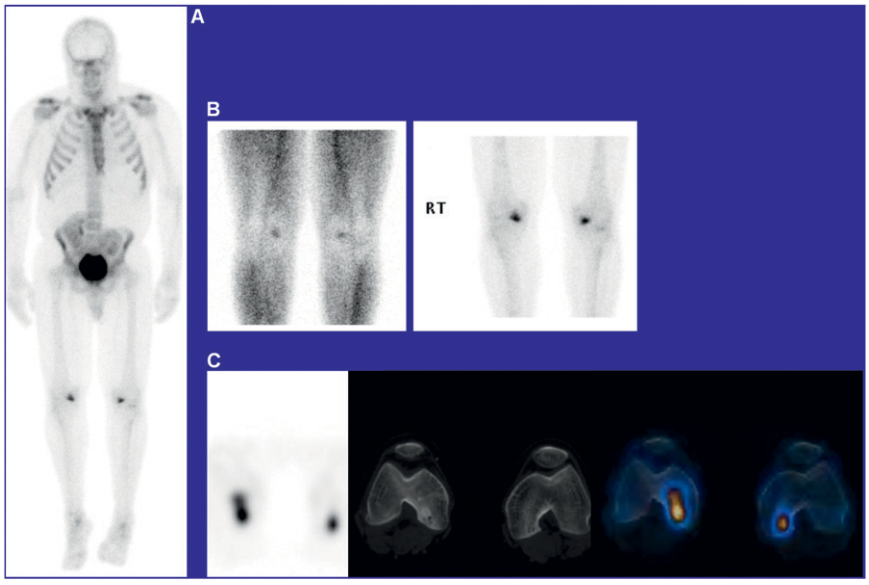

FIGURE 20. Knee pain, steroids, bilateral renal transplants. Left: Whole-body imaging. Top: Blood pool (left) and delayed (right) imaging. Bottom: SPECT (left); CT (middle 2); fused (right 2) images showing uptake consistent with bilateral avascular necrosis.

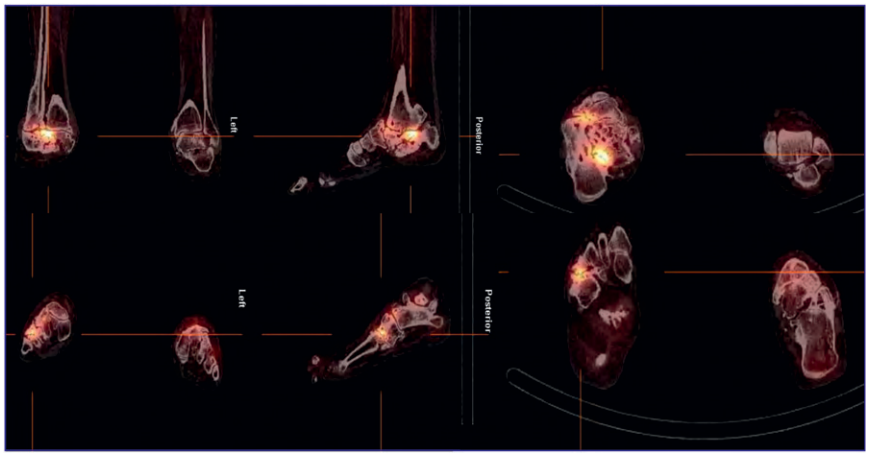

FIGURE 21. SPECT/CT imaging in Charcot foot. Two separate patients (upper, lower). Coronal (left), sagittal (middle), and transverse (right) fused SPECT/CT images with uptake at joint surfaces suggestive of Charcot joint disease.

Kurdziel et al. from the National Institutes of Health (Bethesda, MD) reported on "Temporal characterization of ^{18}F-NaF PET/CT uptake" [459]. They studied 21 patients with multiple myeloma or premyelomatous condition and 24 patients with prostate cancer and known bone involvement or rising prostate-specific antigen. Patients underwent serial torso imaging 3 times over ~60 min and whole-body static imaging at ~2 h after injection. The researchers found a progressive increase in standardized uptake value (SUV) over the 2-h period of observation. They also observed that bone lesions were better identified at later time points. In none of the patients did uptake plateau.

Killeen et al. from the New York–Presbyterian Hospital and the Weill Cornell Medical Center (New York, NY) reported on "The value of SPECT/CT in the setting of a normal ^{111}In-white blood cell [WBC] whole-body planar scintigram" [15]. They studied 188 patients who underwent ^{111}In-WBC whole-body planar scintigraphy. Of these patients, 74 (39%) had normal planar results. Forty-five of the 74 then underwent SPECT/CT; of these, 9 (20%) patients had abnormal uptake, which led to a management change in 7 (16%). Figure 24 shows a 79-y-old man with persistent fever postcystectomy. Whole-body images were interpreted as negative, but SPECT/CT showed definite increased uptake in the pubic symphysis with extension into the adjacent soft tissues.

Heiba et al. from the Mount Sinai School of Medicine (New York, NY) reported on "The beneficial influence of dual-isotope SPECT/CT use on management of patients with suspected diabetic foot infection" [14]. They used 2 radiotracers, ^{99m}Tc-HDP and ^{111}In-WBC, in 191 patients (some patients had marrow studies as well), who underwent 227 SPECT/CT scans. Imaging yielded diagnoses of osteomyelitis in 84 patients, soft tissue infection (STI) in 93, both osteomyelitis and STI in 25, and other bony pathologies in 25. Diagnosis was confirmed by culture/pathology in 66 patients and by follow-up in 161, yielding high sensitivity (98%), specificity (96%), and PPV (99%) and an NPV of 83%. They found that in a large percentage (94%) of the patients scan results directed management (72% to conservative management, 24% to limb salvage procedures, and 4% to major limb amputation). Figure 25 is an example of a patient who had an infection in the large toe and was being evaluated for amputation. SPECT/CT showed that uptake was limited to the distal digit of the large toe; thus surgery was limited to distal digit resection.

^{18}F-FDG Infection Imaging

A number of interesting abstracts at this meeting focused on the use of ^{18}F-FDG for infection imaging. These included presentations on fever of unknown origin (FUO) in adults (4) and children (1), bacteremia (1), fever and neutropenia (2), diskitis (1), and extrapulmonary tuberculosis (1).

Sonoda et al. from Addenbrooke's Hospital (Cambridge, UK) and the Royal Marsden Hospital (London, UK) reported on "Prospective analysis of ^{18}F-FDG PET and ^{111}In-leukocyte scintigraphy in the management of FUO" [1372]. This was a prospective study of 21 patients with FUO. ^{18}F-FDG PET showed a sensitivity of 60%, twice that of ^{111}In-WBC imaging. All patients with positive ^{111}In-WBC studies had positive ^{18}F-FDG PET studies. Figure 26 is an example with a whole-body WBC study that was inter-

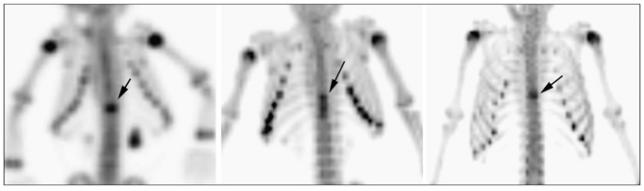

FIGURE 22. Bone scintigraphy with ^{18}F-NaF PET in 3 children with traumatic spine injury. Ages (left to right) were 2, 4, and 19 mo. ^{18}F-NaF PET confirmed equivocal findings and detected new findings of vertebral fracture not seen on skeletal survey.

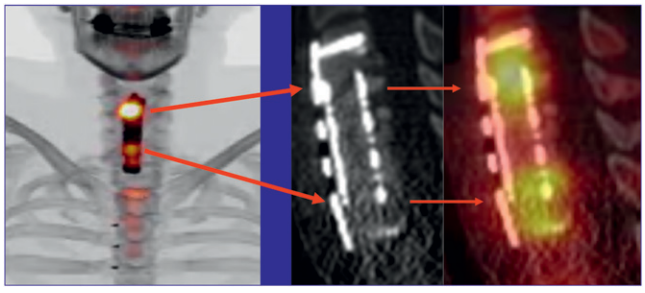

FIGURE 23. ^{18}F-NaF PET/CT and cervical spine fixation hardware. Left: PET/CT maximum-intensity projection (MIP). Middle: CT. Right: Fusion PET/CT. Fused imaging shows abnormal uptake at proximal and distal ends of hardware. Surgical exploration confirmed loosening at these sites.

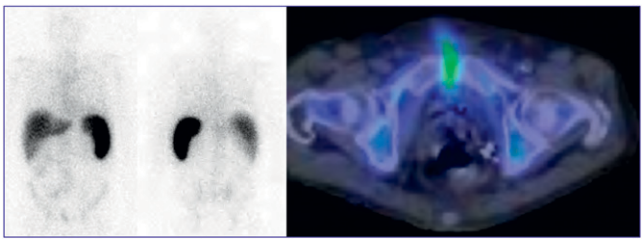

FIGURE 24. 79-y-old man with persistent fever postcystectomy. Left: ^{111}In-white blood cell whole-body planar scintigraphy was interpreted as normal in blinded retrospective study. Right: Fused SPECT/CT showed increased uptake overlying the pubic symphysis with extension into adjacent soft tissues, resulting in a diagnosis of pubic symphysitis.

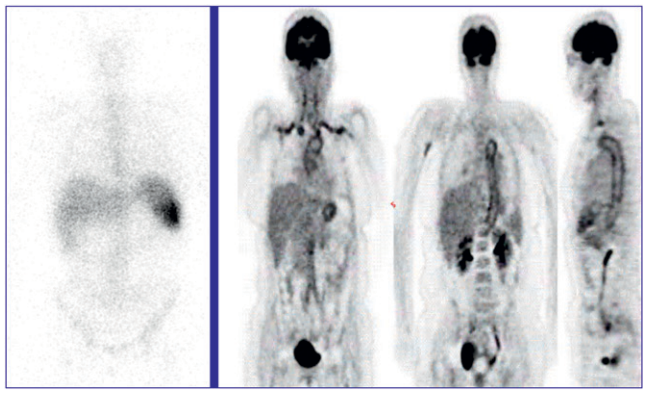

FIGURE 26. Takayasu arteritis. Left: ^{111}In-white blood cell imaging interpreted as negative. Right: ^{18}F-FDG PET shows definite FDG uptake consistent with large vessel arteritis.

preted as negative, whereas ^{18}F-FDG PET showed definite intense uptake in large vessels, consistent with the final diagnosis of Takayasu arteritis. Figure 27 shows a patient with tuberculosis who had a negative ^{111}In-WBC study but an ^{18}F-FDG PET study that showed multiple sites of uptake in the mediastinum and typical nodal areas.

Kubota et al. from the National Center for Global Health and Medicine (Tokyo, Japan) and a consortium of Tokyo academic medical centers reported on "FDG PET for the diagnosis of FUO: a Japanese multicenter study" [16]. This was a retrospective study that included 81 patients with FUO from 6 institutions. Overall sensitivity of ^{18}F-FDG PET was 81% and specificity was 75%, with a PPV of 88%. They reported a sensitivity of 89% for infection, 100% for tumor/granuloma, and a specificity of 84% in patients classified as other or unknown (arthritis/vasculitis/collagen disease). They found that in ~75% of patients studied, PET provided additional unexpected information.

London et al. from the Children's Hospital at Westmead and Sydney University Medical Center (Australia) reported on "FDG PET/CT for investigation of pyrexia of unknown origin, inflammatory and infective conditions in children" [1398]. The study included 69 patients who underwent 84 scans. Researchers found an occult inflammatory focus in 50% of the patients. PET/CT was particularly useful in immunocompromised patients. It guided biopsy and positively affected management. Among the diagnoses facilitated by PET/CT in this group were multifocal osteomyelitis, bowel graft-versus-host disease, great vessel vasculitis, disseminated Epstein-Barr virus infection, and fungal infection in chronic granulomatous disease.

Nanni et al. from the Policlinico S. Orsola-Malpighi and the Istituti Ortopedici Rizzoli (Bologna, Italy) reported that "FDG PET/CT is useful for interim evaluation of response to therapy in patients affected by diskitis" [1375]. The study included 9 patients classified as early responders. They had significant decreases in SUV_{max} very soon after initiation of appropriate treatment. Three patients referred to as nonresponders had no decrease in SUV_{max} after initiation of therapy, so a different and more effective therapy was initiated, leading to decreased uptake similar to that of early responders (Fig. 28).

Chien et al. from the Johns Hopkins University (Baltimore, MD) reported that "Low-dose propranolol is effective in suppressing FDG brown adipose tissue uptake in pediatric patients: qualitative and quantitative analyses" [400]. Prior to the year 2010, patients did not receive propranolol and were used as controls; subsequently most patients received the drug prior to the study. Figure 29 shows a 16-y-old girl with Hodgkin lymphoma who, when first imaged with ^{18}F-FDG PET in 2009 had considerable brown fat uptake, and the same patient a year later pretreated with low-dose propranolol, showing no brown fat uptake. Qualitative

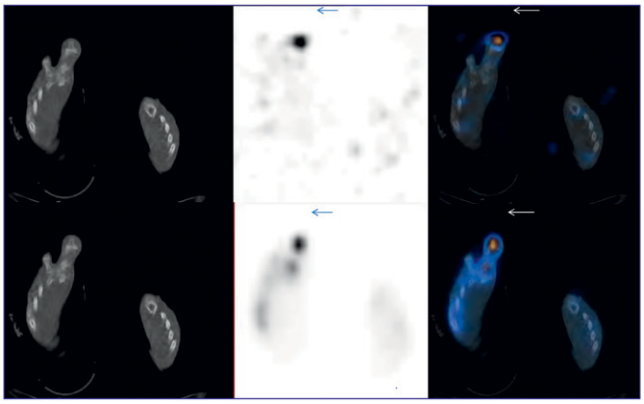

FIGURE 25. Right large toe distal phalanx osteomyelitis in a diabetic patient. Left: CT. Middle: White blood cell SPECT transverse (top). Right: Fused SPECT/CT shows uptake in distal digit of first toe.

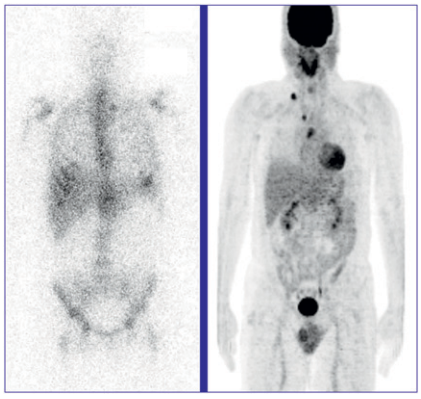

FIGURE 27. Tuberculosis. Left: ^{111}In-white blood cell imaging. Right: ^{18}F-FDG PET.

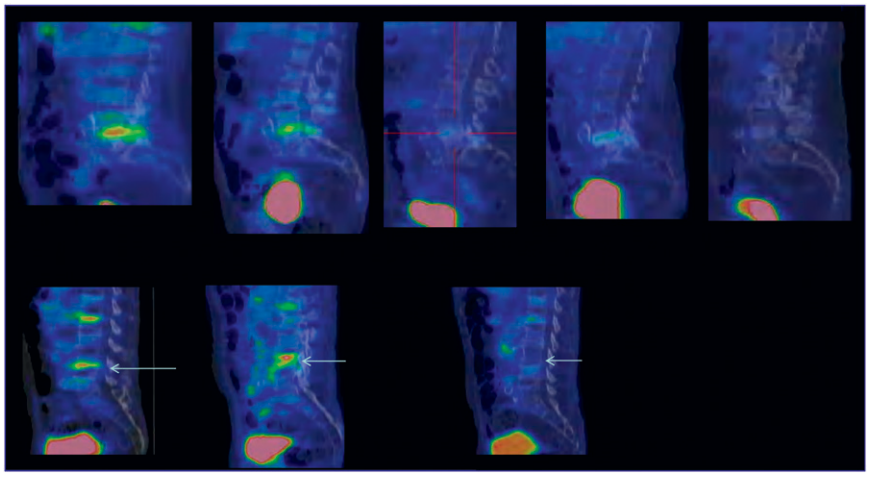

FIGURE 28. PET/CT for interim evaluation of response to therapy in diskitis. Top row: images from early responder. Left to right: March 2010, baseline, SUV_{max} = 7; April 2010, after initiation of therapy, SUV_{max} = 3.9; Jul 2010, negative; August 2010, negative; September 2010, negative. Bottom row: images from nonresponder. Left to right: May 2010, baseline, SUV_{max} = 4.8; June 2010, SUV_{max} = 6.3; July 2010, SUV_{max} = 2.3 after switch to alternative therapy.

and quantitative analyses demonstrated significantly lower ($P < 0.0001$) FDG uptake in patients pretreated with propranolol.

Radioiodine Thyroid Cancer

A number of presentations looked at the utility of SPECT/CT in radioiodine thyroid cancer diagnosis. Wong et al. from the University of Michigan Hospital and Veterans Affairs Ann Arbor Healthcare reported on the "The role of diagnostic ^{131}I planar and SPECT/CT in staging and treatment of thyroid cancer patients" [1354]. They studied 100 patients (71 women, 29 men; mean age, 45 y) with differentiated thyroid cancer. Patients received 1 mCi (37 MBq) ^{131}I and underwent planar and SPECT/CT studies. SPECT/CT found additional neck metastases in 14 and distant metastases in 6 patients. SPECT/CT upstaged 17% of patients compared with initial postoperative staging. Figure 30 is an example of 2 different patients with focal uptake in the neck that look quite similar on whole-body planar imaging. SPECT/CT shows that the focal uptake in one patient fuses with nodes in the neck as a result of regional metastases, whereas in the other patient the FDG uptake fused to the submandibular gland and was benign.

Agrawal et al. from the Post Graduate Institute of Medical Education and Research (Chandigarh, India) reported on "Post-therapy ^{131}I SPECT/CT in risk stratification and management of patients with differentiated thyroid cancer: a prospective study." They imaged 38 consecutive patients with SPECT/CT after thyroidectomy. They found a change in nodal status from N0 to N1 or higher in 13% of patients, and the results of imaging changed management in 14 (39%) patients and risk classification in 5 (13%) patients. Figure 31 is an example of a ^{131}I whole-body scan 8 d after 120 mCi ^{131}I for papillary thyroid cancer. The scan shows a high tumor-to-background ratio and little anatomic information. With the SPECT/CT the FDG uptake corresponded to paratracheal nodes, and the patient was upstaged from M0 to M1 disease.

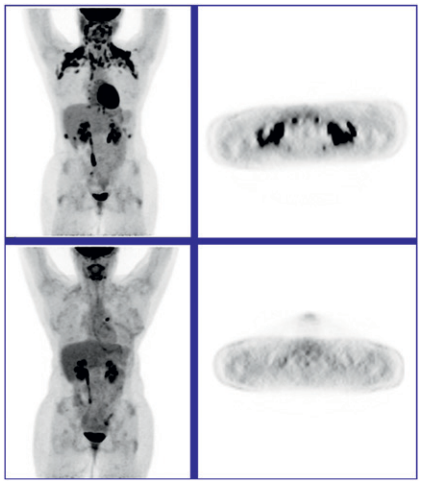

FIGURE 29. Suppressing brown fat uptake. 16-y-old girl with Hodgkin lymphoma imaged (top) without and (bottom) 1 y later with low-dose propranolol.

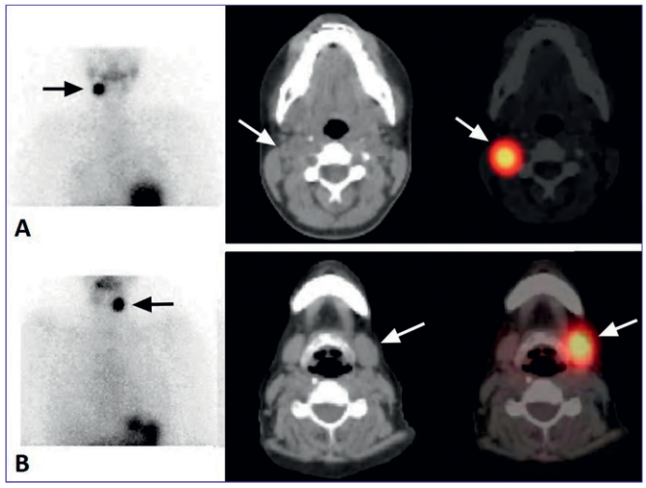

FIGURE 30. (A) Patient with papillary thyroid cancer (PTC) status postthyroidectomy underwent diagnostic ^{131}I SPECT/CT. Focal uptake in right submandibular region on planar images was suspicious for nodal disease (arrow). SPECT/CT showed an enlarged right cervical level II lymph node with focal ^{131}I uptake (arrows). (B) Another patient with PTC treated with thyroidectomy and ^{131}I for thyroid remnant ablation returned for surveillance imaging 1 y after surgery. Planar images showed focal uptake in left submandibular region (arrow). SPECT/CT localized focal uptake to normal left submandibular gland, representing asymmetric physiologic uptake (arrows).

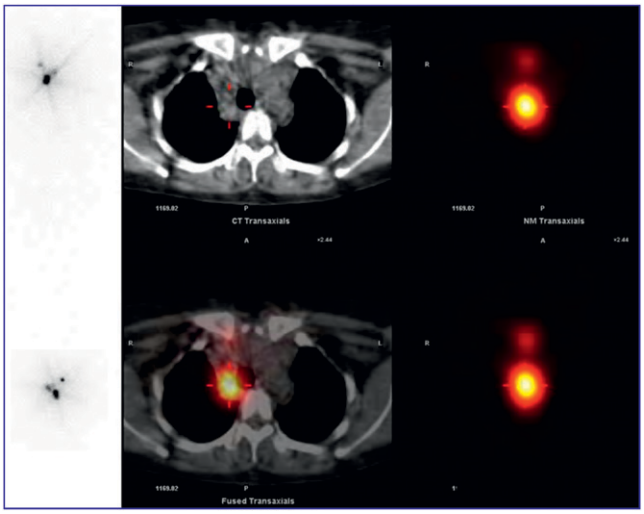

FIGURE 31. 59-year-old woman referred for high-dose radioiodine therapy after thyroidectomy for papillary thyroid cancer. Left: Planar whole-body scintigraphy 8 d after administration of 120 mCi ^{131}I showed multiple foci of increased tracer uptake in neck. Right: SPECT/CT of neck and chest localized uptake to right lower paratracheal lymph nodes, changing stage from M0 to M1.

Liu et al. from Sichuan University (Chengdu, China) reported on "Lung absorbed dose in radioiodine therapy of thyroid cancer with diffuse pulmonary metastases" [180]. The study included 10 patients with diffuse thyroid cancer lung metastases who underwent serial ^{131}I whole-body quantitative scans. The researchers calculated the median ^{131}I uptake in lungs at 24 h at 5.0% (range, 1%–37%), the median effective half-life in the lungs as 33 h (range, 15–107 h) and body as 16 h (range, 8–25 h), and lung absorbed dose as 0.03–1.11 mGy/MBq. Based on the empiric-fixed-activity method, they concluded that the risk of radiation-induced pneumonitis/pulmonary fibrosis is low in patients with ^{131}I thyroid therapy with doses of 7.4 GBq (200 mCi) for diffuse lung metastases.

Neuroendocrine Tumor Imaging

A number of scientific presentations at this meeting focused on neuroendocrine tumor (NET) imaging using a variety of pharmaceuticals: ^{111}In-pentetreotide (3), ^{18}F-DOTANOC (5), ^{18}F-DOTATOC (3), ^{18}F-DOTATATE (2), ^{18}F-FDG (2), ^{18}F-DOPA

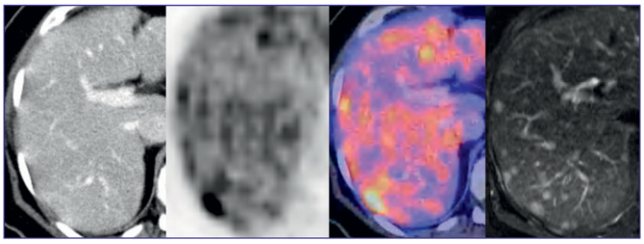

FIGURE 32. Comparative detection of liver metastases. Images acquired in a 62-y-old patient with ileal carcinoid and hepatic metastases. Left to right: CT, PET, PET/CT, and MR transverse images.

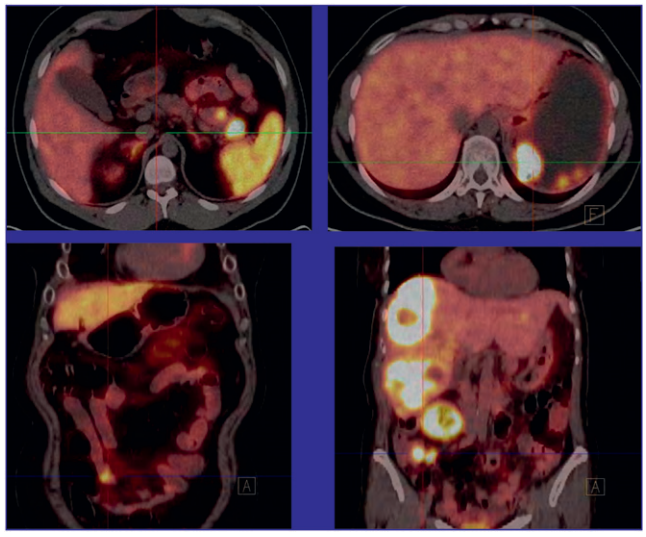

FIGURE 33. Primary tumors detected with ^{68}Ga-DOTATATE PET/CT in (top left) pancreas, (top right) stomach, (bottom left) small intestine, (bottom right) colon.

(3), and ^{99m}Tc-HYNIC octreotide (1). Pfannenberg et al. from the Eberhard-Karls University (Tübingen, Germany) reported on "Comparison of ^{68}Ga-DOTATOC PET/CT and whole-body MRI in staging of neuroendocrine tumors" [126]. The study included 51 patients with histologically proven NETs and suspected metastases. All patients underwent multiphase contrast CT, ^{68}Ga-DOTATOC PET/CT, and whole-body MR imaging. Consensus diagnoses were based on imaging, surgery, histology, and follow-up. Forty-one (80%) of the patients had 593 metastatic lesions, 22 of which were found only with ^{68}Ga-DOTATOC-PET/CT, 11 only with CT, and 47 only with whole-body MR imaging. ^{68}Ga-DOTATOC PET/CT and whole-body MR had comparable overall detection rates (91% and 92%, respectively) for metastatic involvement but differed in organ-based detection rates. PET/CT had significantly higher sensitivity than MR in detecting metastatic lymph nodes (100% and 73%, respectively) and pulmonary lesions (100% and 87%, respectively), whereas whole-body MR had significantly higher detection rates than PET/CT for liver (99% and 92%, respectively) and bone (96% and 82%, respectively) metastases. Figure 32 is an example of a 62-y-old patient with ileal carcinoid and hepatic metastases, showing the relative abilities of CT, PET, PET/CT, and MR imaging in detection of liver metastases, with MR typically having the best definition.

Ambrosini et al. from the S. Orsola-Malpighi Hospital (Bologna, Italy) reported on ^{68}Ga-DOTANOC PET/CT accuracy for neuroendocrine lesion detection: the Bologna experience" [1298]. The study included 204 patients with known (188) or suspected (16) NETs. The researchers found an overall sensitivity of 87% and a specificity of 95%, with PPV of 96% and NPV of 84%.

Kunikowska et al. from the Medical University of Warsaw (Poland) and the Institute of Atomic Energy (IAE) POLATOM (Otwock-Swierk, Poland) reported on "Usefulness of PET/CT investigations with ^{68}Ga-DOTATATE in NETs in diagnosis of primary tumors" [1355]. The study included 277 patients with NETs. ^{68}Ga-DOTATATE PET/CT detected 51 (80%) of 64 primary tumors (6 in lungs; 21 in pancreas, where 2 were seen with

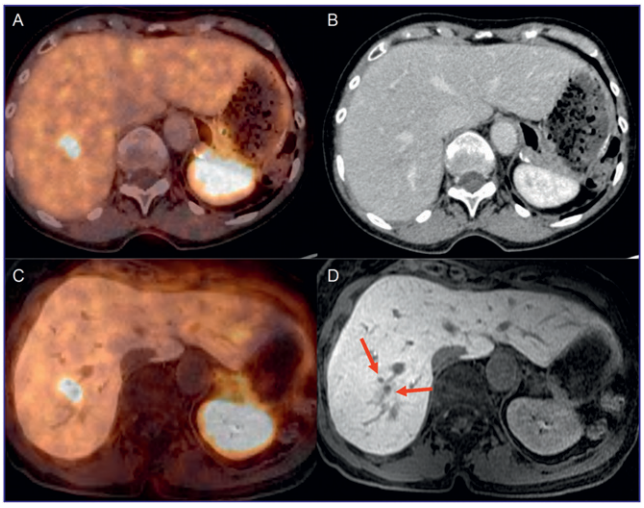

FIGURE 34. PET/MR fusion for detection of neuroendocrine tumor liver metastases. Top: ^{68}Ga-DOTATOC fused PET/CT (left) and contrast CT (right). Lesion is not seen on CT. Bottom: ^{68}Ga-DOTATOC fused PET/MR (left) and MR (right). Tumor is seen on MR.

CT alone; 23 in intestines, where 3 were seen with CT alone; 1 in stomach; and 1 in pelvis). Both ^{68}Ga-DOTATATE PET/CT and CT with contrast media failed to find 13 (20%) of the 64 primary tumors. Figure 33 shows fused PET-CT examples from this study of primary tumors found in the pancreas, stomach, small intestine, and colon.

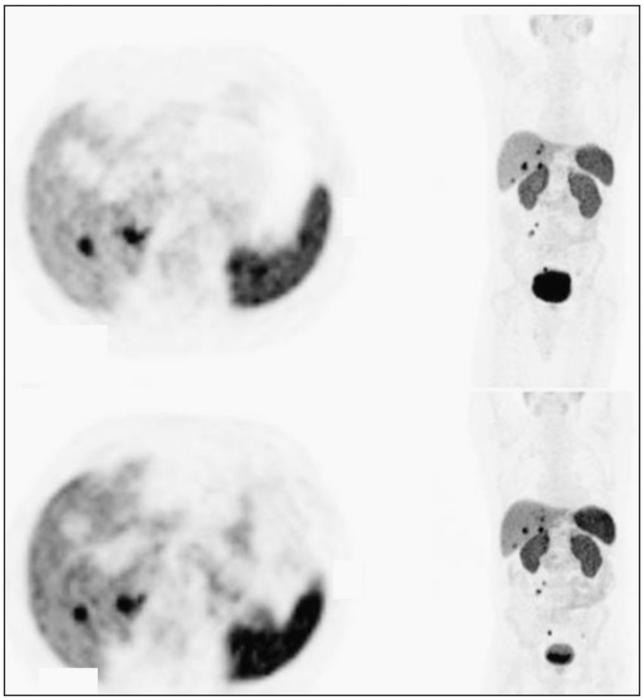

FIGURE 35. Left: SPECT. Right: planar whole-body imaging. Top: Imaging with octreotide (Sandostatin) treatment. SUV_{max} in tumor = 33, liver = 10, spleen =20. Bottom: imaging with no octreotide treatment: SUV_{max} in tumor = 32, liver = 12, spleen = 25. Higher liver and spleen uptake without octreotide. Tumor uptake unchanged.

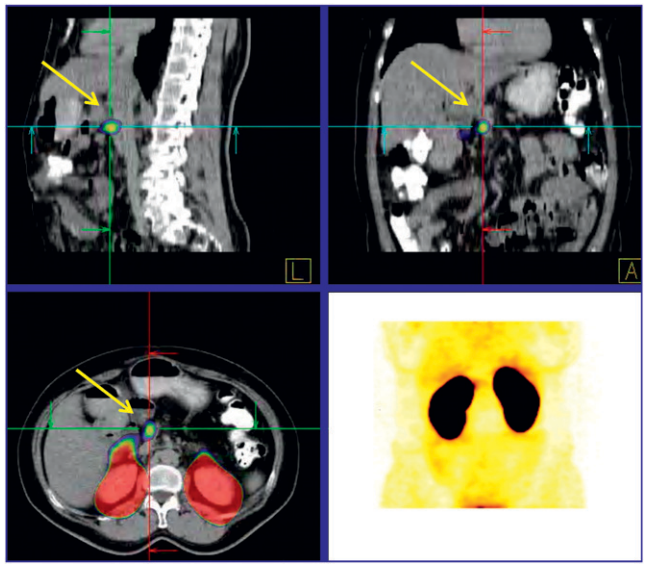

FIGURE 36. 62-y-old woman with hypoglycemia in whom SPECT/CT, MR, and somatostatin receptor scintigraphy were negative but $Lys^{40}NH_2$(Ahx)-HYNIC-^{99m}Tc imaging clearly showed focal uptake in the insulinoma.

Prasad et al. from the Zentralklinik Bad Berka (Germany) and University Hospital Jena (Germany) reported on "Detection of unknown primary in patients with NETs using ^{68}Ga-somatostatin receptor PET/CT: results in 129 patients" [1347]. All patients had histopathologically documented NETs (100 well- and moderately well-differentiated and 29 poorly or undifferentiated). They used a variety of ^{68}Ga-labeled radiopharmaceuticals (DOTATATE, DOTATOC, DOTANOC) and found a 58% detection rate for primary tumors.

Schreiter et al. from Charité Berlin (Germany) and Kochi University (Japan) reported on "Evaluation of PET-MRI fusion for the detection of NET liver metastases" [564]. Their results showed that in 22 patients with 181 lesions, retrospectively fused PET/MR imaging had higher sensitivity, specificity, PPV, and NPV (91%, 96%, 97%, and 87%, respectively) than ^{68}Ga-DOTATOC PET/CT (74%, 88%, 93%, 69%, respectively) or gadolinium-EOB-DTPA MR imaging (88%, 87%, 93%, 83%, respectively). Figure 34 is an example in which a lesion is not

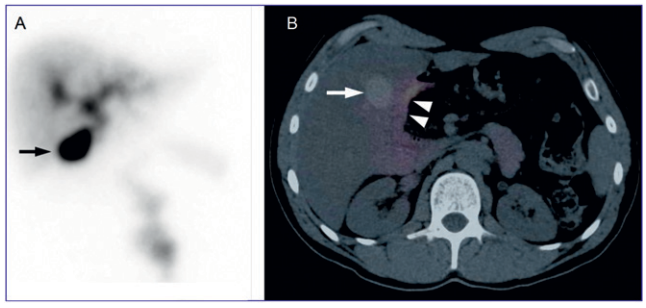

FIGURE 37. (A) Planar hepatobiliary iminodiacetic acid image was uncertain, thought likely to be gallbladder filling. (B) SPECT/CT localized activity to the duodenum. There was no gallbladder filling.

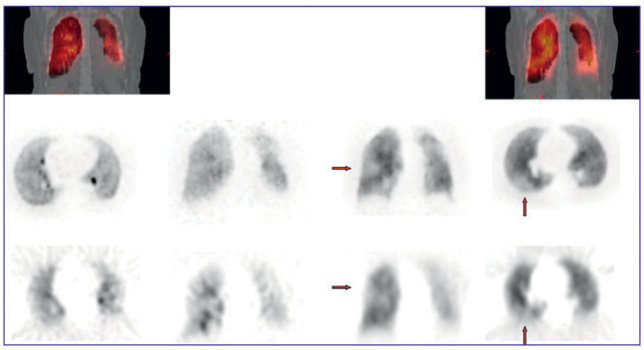

FIGURE 38. PET lung ventilation/perfusion imaging. Top rows: Ventilation and perfusion posterior images. Middle and lower rows: Ventilation/perfusion mismatch in the right lung with normal ^{68}Ga-aerosol (left) and perfusion defect with ^{68}Ga-macroaggregated albumin (MAA; right) (red arrows). Bottom row: ^{99m}Tc-aerosol and ^{99m}Tc-MAA imaging acquired 3 d later.

seen on ^{68}Ga-DOTATOC PET/CT but is visible on ^{68}Ga-DOTATOC PET/MR imaging.

Haug et al. from Ludwig-Maximilians University (Munich, Germany) reported that "Treatment with long-acting octreotide does not reduce tumor uptake of ^{68}Ga[DOTA$_0$, Tyr$_3$] octreotate in patients with NETs" [122]. They studied tracer uptake in 105 patients on and off therapeutic octreotide (Sandostatin) and showed that the amount of uptake in liver and spleen decreased with Sandostatin but that in tumors there was no statistical difference in the amount of uptake. Figure 35 shows an example with and without octreotide, indicating decreased uptake in liver tissues with octreotide therapy, as confirmed by SUV_{max} measurements.

An interesting but small study came from Hubalewska-Dydejczyk et al. from Jagiellonian University Medical College (Krakow, Poland) and IAE Radioisotope Centre POLATOM (Otwock-Swierk, Poland), who reported on ^{99m}Tc-labeled GLP-1 scintigraphy with the use of [Lys^{40}NH$_2$(Ahx)-HYNIC-^{99m}Tc]-exendin-4 in insulinoma localization" [561]. The study included 5 patients, in each of whom the researchers were able to visualize localization. Figure 36 is a 62-y-old woman with hypoglycemia in whom CT, MR, and somatostatin receptor scintigraphy were negative but Lys^{40}NH$_2$(Ahx)-HYNIC-^{99m}Tc imaging clearly showed an insulinoma.

Kamphuis et al. from Erasmus University Medical Center (Rotterdam, The Netherlands) reported on "Somatostatin receptor scintigraphy in sarcoidosis" [341]. The study included 218 patients with sarcoidosis who underwent imaging with ^{111}In-pentetreotide. Researchers found uptake in 100% of those with X-ray stages for sarcoidosis of 1, 2, 3, and 4, but in only 52% of patients with X-ray–based stages 0. Of the 49 patients in this latter group, 36 had lung biopsies and 31 of these were found to have non-necrotizing granulomas.

Markelewicz et al. from the Harvard Medical School and Children's Hospital Boston (MA) reported on "Radiation exposure to caregivers of pediatric neuroblastoma patients undergoing ^{131}I-MIBG therapy" [403]. They wanted to evaluate the relationship between administered activity and caregiver radiation exposure. The study included 14 children (ages 3–13 y) with relapsed neuroblastoma who were treated on a weight-based dosing scheme. Patients were in hospital isolation for 3–5 d. Caregivers were designated (usually parents) and received specific radiation safety training and instructions from the nursing staff on providing care (emptying urine, feeding, medications). Caregivers had whole-body radiation monitoring. Results showed no significant difference in caregiver radiation exposure (0.35–3.8 mSv) relative to the wide range of patient administered activities (5.9–23.3 GBq) or by patient age ($<$ or $\geq$ 7 y). All caregivers received radiation allowed under current regulations for individuals exposed to patients ($<$5.0 mSv).

Arabi et al. from the University of Michigan (Ann Arbor) reported on "Utilization of SPECT/CT for evaluation of suspected acute cholecystitis in problematic cases" [1362] and on intra- and interobserver variability assessment compared to planar hepatobiliary iminodiacetic acid (HIDA) imaging. The investigation included 1,035 HIDA studies. Of these, only 55 (5%) patients underwent SPECT/CT, performed only if the planar study was indeterminate or discordant with the clinical condition. SPECT/CT led to a change in interpretation in 22 (41%) of these patients, with determination going from normal to abnormal in 28% and abnormal to normal in 13%. Causes of discordance proved to be superimposed bowel activity (18), altered gallbladder anatomy (2), and cystic duct sign (2). Figure 37 shows a HIDA planar image with apparent gallbladder filling; however, SPECT/CT shows the activity fused with the duodenum and that the gallbladder had not filled.

A small but interesting study was presented by Ament et al. from University Medical Center Mainz (Germany) on "PET lung ventilation/perfusion imaging using ^{68}Ga-labeled aerosol (Galligas) and ^{68}Ga-labeled macroaggregated albumin [MAA]" [343]. Figure 38 is an example with a ventilation/perfusion mismatch in the right lung with ^{68}Ga-aerosol and ^{68}Ga-MAA (red arrows) and, 3 d later, with ^{99m}Tc-aerosol and ^{99m}Tc-MAA. They both showed mismatched normal ventilation and lung perfusion defects.

Codreanu et al. from Children's Hospital of Philadelphia (PA) reported on "Comparison of gastroesophageal reflux [GER] scintigraphy at 5-s and 60-s frame acquisition" [1399]. Figure 39 shows no evidence of reflux in the 60-s frame acquisition but

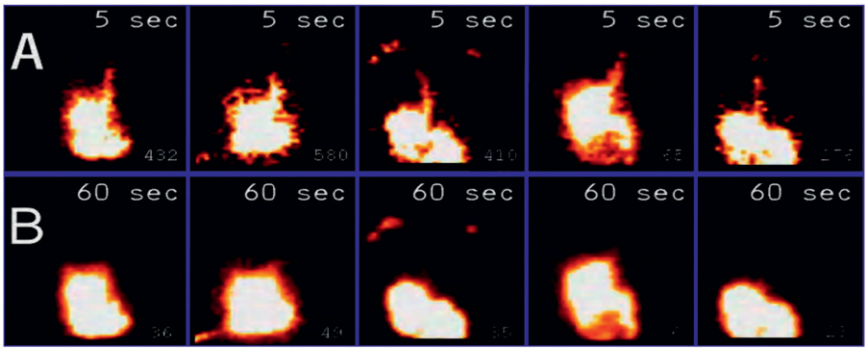

FIGURE 39. Examples of high-grade gastroesophageal reflux detected on (A) 5-s frames but not visualized on (B) 60-s frames.

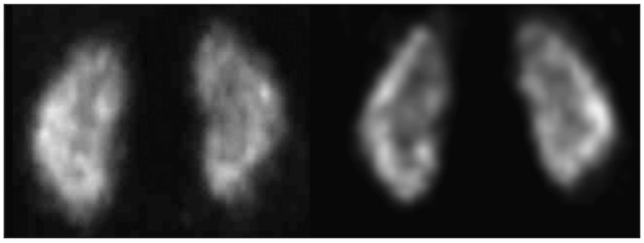

FIGURE 40. Parallel-hole (left) and pinhole (right) ^{99m}Tc-DMSA SPECT in the same patient with same acquisition time and at same slice level. Pinhole SPECT was believed to be superior.

shows reflux events in the 5-s acquisition rate. This study indicated a significant increase in sensitivity (0.001) for detection of reflux using the 5-s acquisition frame. Ten (20%) patients had high-level GER episodes detected only with the 5-s acquisition technique.

Drubach et al. from Children's Hospital (Boston, MA) reported on "Posterior view versus the geometric mean for gastric emptying calculation in children" [1393]. They showed that in children younger than 8 y that posterior-only acquisition is sufficient for accurate calculation of 1-h gastric emptying but that in older patients the geometric mean calculation is recommended.

Demonceau et al. from St. Elizabeth Hospital (Zottegem, Belgium) and Université Catholique de Lovain (Brussels, Belgium) reported on "Pinhole SPECT and parallel-hole SPECT comparison in children's kidneys studied with ^{99m}Tc-DMSA" [1404]. The study included 8 patients. Figure 40 is an example of a parallel-hole SPECT and pinhole SPECT study in the same patient with the same acquisition time and approximately the same coronal slice. The authors found that with pinhole SPECT they could achieve better visualization of the Bertin columns and better definition of the borders of the cortex. Although proven defects were detected equally by the 2 methods, they were sharper with pinhole SPECT. Pinhole SPECT reduced the number of equivocal results and was associated with a superior degree of confidence.

Glass et al. from Medical Imaging of Southern California and Lymphedema Center of Santa Monica (CA) reported on the "Role of lymphoscintigraphy of the legs in obesity" [509]. They studied the etiology of swelling in large patients. The study included 65 patients with high body mass indices referred with swollen legs. The researchers looked particularly at the incidence of dermal backflow as seen in patients with lymphedema (Fig. 41). They found that lymphoscintigraphy was effective in all cases in assessing the etiology of leg enlargement.

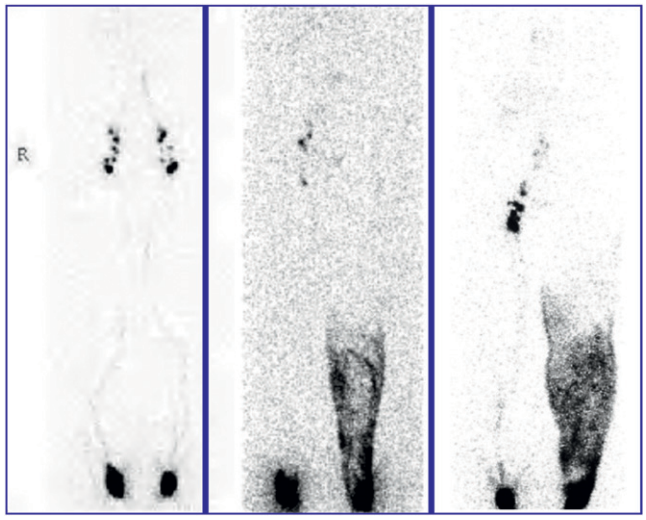

FIGURE 41. Lymphoscintigraphy to assess etiology of leg enlargement and incidence of dermal backflow in patients with high body mass indices. Patient with lipidema (normal) (left). Patients with primary (middle) and secondary (right) lymphedema (dermal backflow pattern).

I will conclude by encouraging all those with an interest in general nuclear medicine to join the General Clinical Nuclear Medicine Council. Thank you.

Harvey A. Ziessman, MD
Johns Hopkins University
Baltimore, MD